Supplementary Materials for

MYC Regulates the Anti-Tumor Immune Response through CD47 and PD-L1

Stephanie C. Casey, Ling Tong, Yulin Li, Rachel Do, Susanne Walz, Kelly N. Fitzgerald, Arvin Gouw, Virginie Baylot, Ines Gutgemann, Martin Eilers, Dean W. Felsher*

*Corresponding author. Email: dfelsher@stanford.edu

This PDF file includes:

Materials and Methods

Transgenic mice

Animals were identically raised and housed at Stanford University; immunocompromised mice were maintained on Bactrim chow. The Tet-off system transgenic lines used for conditional MYC expression and oncogene addiction have been previously described *(1, 3, 46)*. *Eμ-tTA/tet-O-MYC* mice develop lymphoma/leukemia (MYC T-ALL) and *LAP-tTA/tet-O-MYC* mice develop HCC (MYC HCC). RAG1 KO mice on an FVB background were generously provided by Lisa Coussens. Genotyping was performed using genomic DNA from animal tails. All experiments were approved by the Administrative Panel on Laboratory Animal Care (APLAC) at Stanford University in accordance with institutional and national guidelines. For transgenic primary tumors, a minimum of 3 mice were used per treatment condition group. Male mice were used for all transgenic mouse experiments and tumors arose at approximately 2-3 months of age.

Cell culture

Hematopoietic tumor cell lines (MYC T-ALL 4188 cells derived from the transgenic mouse model, human P493-6, human T-ALL Jurkat, and human T-ALL CCRF-CEM) were grown in RPMI 1640 supplemented with 10% FBS, 1% penicillin/streptomycin, 50 μM 2-mercaptoethanol at 37°C in 5% CO_2. Solid human tumor cell lines (H1299, SKMEL28), mouse MYC HCC, and human HEPG2 were grown in DMEM supplemented with 10% FBS and 1% penicillin/streptomycin at 37°C in 5% CO_2. To turn off expression of the *MYC* transgene, cells were treated with 20 ng/mL Dox. Primary human T-ALL cells were obtained from four deidentified patient samples and were cultured as previously described *(47)*. Briefly, cells were cultured in StemSpan H3000 (StemCell) supplemented with human stem cell factor (50 ng/ml), human IL-7 (20 ng/ml), human IL-3 (20 ng/ml), and human FLT3 ligand (20 ng/ml) (Peprotech). Human cell lines were purchased from ATCC.

Overexpressions and knockdowns

For forced expression of CD47 and PD-L1, cDNAs were cloned in to MSCV-Hygro or MSCV-Puro backbones. The plasmids (CD47, PD-L1, or empty control MSCV) were transfected into 293T cells and virus-containing medium supernatants were used to infect tumor cells using polybrene methodology. Infected cells were selected, expanded, forced expression confirmed, and prepared for injection. For forced expression, one cohort was collected at day 0 and day 4 after turning MYC "off" with doxycycline. These tissues were used for gene expression analysis and immunostaining. Another, separate cohort was followed for survival analysis.

shRNA-mediated knockdowns were performed with the pLKO.1 lentiviral vector containing either control, CD47, or PD-L1-specific shRNA. shRNA-mediated knockdown of human MYC was performed with the pLKO.1 lentiviral vector containing a scrambled control or MYC shRNA (Sigma). PD-L1 shRNA on a pLKO.1-puro backbone was purchased from Sigma and CD47 shRNA (Sigma) was cloned into a pLKO.1-Hygro backbone (Addgene). The plasmids were transfected into packaging cells and virus-containing medium supernatants were used to infect tumor cells using polybrene methodology. For conditional knockdowns, stable cell lines were generated and the time course following MYC inactivation with 20 ng/mL Dox is indicated. For stable knockdowns, the time course is indicated as the time post-viral infection.

Tumor growth assays

10 x 10^6 tumor cells were injected subcutaneously in a volume of 100ul into 4-6 week old female FVB animals and were allowed to form tumors of 1.5 cm in diameter. At that time, mice were either euthanized and tissues collected or treated with Dox in their drinking water (100 μg/mL final concentration).

Reconstitutions of RAG1 KO mice

4-6 week old female FVB RAG1 KO mice were injected intravenously with 4 x 10^6 purified $CD4^+$ T cells that had been magnetically enriched from CAG-luc-eGFP L2G85 mice (Miltenyi Biotec beads and columns). Tumor cells were injected one week after reconstitution.

In Vivo bioluminescence imaging

Bioluminescence imaging was performed as previously described *(13)*. Briefly, cell lines (Fig. 4) were infected with pMSCVneo containing fLuc. For fLuc immune labeling, see Reconstitutions of RAG1 KO mice above. Mice were anesthetized with inhaled isoflorane/oxygen using the Xenogen XGI-8 5-port Gas Anesthesia System. d-luciferin (150 mg/kg) was injected intraperitoneally 10 min prior to imaging. Animals were placed into the light-tight chamber and were imaged with an IVIS-200 cooled CCD camera (Xenogen). Living Image (Xenogen) was used to collect and analyze data and generate pseudocolor images.

RNA isolation, cDNA preparation, and qPCR

All tissues and cells were flash-frozen in liquid nitrogen and stored at -80°C until RNA preparation. RNA was isolated using the TRIzol Reagent (Invitrogen) according to manufacturer instructions. cDNA was synthesized using SuperScriptIII (ThermoFisher). qPCR was performed using specific primers (Table S1) and the SYBR Green qPCR Kit (Roche) in an Applied Biosystems Real-Time PCR System (Life Technologies) with QuantStudio12K Flex Software. Data was analyzed using the cycle threshold method (normalized to *UBC)*. A minimum of 3 biological and 3 technical replicates were used for all qPCR experiments.

Lymphocyte analysis and flow cytometry

Tissues were manually dissociated between microscope slides and strained to remove debris. Lysis buffer (0.15 M NH_4Cl, 10 mM $KHCO_3$, 0.1 mM EDTA pH 7.3) was used to remove red blood cells. Cells were washed and resuspended in cold flow cytometry buffer (1% FBS, 0.1% sodium azide in PBS). Staining was performed according to manufacturer instructions with the indicated antibodies (eBioscience). Labeled cells were analyzed on a FACSCalibur (Becton Dickinson), and data was analyzed using FlowJo (Treestar). Each plot is representative of three or more animals. Annexin-V and 7-AAD were used according to manufacturer's protocol (eBioscience).

Immunohistochemistry and immunofluorescence

Immunohistochemistry and immunofluorescence were performed as previously described *(13)*. Briefly, senescence-associated β-galactosidase staining was performed on tissue sections that had been embedded in OCT freezing medium (Tissue Tek) and stored at -80°C. Tissue sections were warmed to room temperature, fixed in 0.5% glutaraldehyde in PBS, and washed in PBS pH 5.5.

Sections were stained for 8 h in a solution containing 250 mM potassium ferricyanide, potassium ferrocyanide, and $MgCl_2$ in PBS pH 5.5, mounted in 50% glycerol/PBS and promptly imaged.

CD31 staining was also performed on frozen sections. Briefly, slides were thawed, fixed in acetone, blocked in Dako serum-free blocking reagent, incubated in rat anti-mouse CD31 (1:50, BD Pharmingen) for 1.5 hours at room temperature, incubated with anti-rat biotinylated IgG (1:300) and Cy3-streptavidin (1:300) for 30 min at room temperature), and counterstained with DAPI.

CC3, PH3 (Cell Signaling), F4/80 (Invitrogen), CD69 (AbCam), CD47, and PD-L1 (R&D Systems) primary antibodies were used according to manufacturer recommendations. Tumors were fixed in 4% paraformaldehyde, embedded in paraffin, and sectioned. Sections were stained as previously described *(4)*. CD47, PD-L1, CC3, and PH3 stainings were counterstained with DAPI and CD69 and F4/80 stainings were counterstained with hematoxylin.

Pictures were taken with 20-40x objectives on a Leica DMI6000 microscope with LASAF software. At least 5 random fields per section and at least 3 tumors per experimental condition were imaged.

ChIP

ChIP-sequencing reads were aligned to the murine mm9 or the human hg19 reference genome using Bowtie v0.12.7 and binding traces were obtained using MACS v1.4.2. To allow comparisons across samples, all files were normalized to the same number of mappable reads. Binding profiles were visualized using the Integrated Genome Browser software *(48)*.

Nuclear run-on

The nuclear run-on assay was performed as previously reported *(49-51)*. Briefly, P493-6 nuclei were isolated using cell lysis buffer. The nascent RNA was labeled with Biotin-UTP. Total nuclear RNA was purified with the Qiagen RNeasy kit. Capture of Biotin-labeled nascent RNA was followed by cDNA synthesis, cRNA synthesis, and cRNA purification (Ambion TotalPrep RNA Amplification) before hybridization to the Affymetrix microarray platform.

Correlation of gene expression in human tumors

Correlation of MYC expression with immune-related surface receptors was determined using the R2 platform (R2: Genomics Analysis and Visualization Platform (http://r2.amc.nl)) with datasets for human liver *(52)*, kidney *(53)*, and colon tumors *(54)*. For each gene, one highly expressed probe was used to determine the Pearsons correlation coefficients and *P*-values.

Statistics

Differences between groups were analyzed using one-way ANOVA with a Tukey's post hoc test. A logrank test was performed for survival analysis (Fig. 4A). $P < 0.05$ was considered to be significant and is indicated by one asterisk (*). $P < 0.01$ is indicated by two asterisks (**). $P < 0.001$ is indicated by three asterisks (***). Graphs are presented as the mean ± SEM. Analyses were performed with GraphPad Prism, version 5 (GraphPad Software).

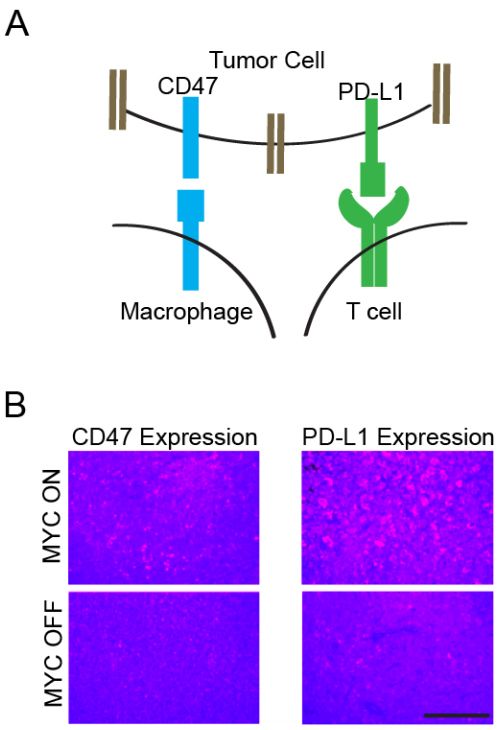

Fig. S1

CD47 and PD-L1 are two important immune regulatory molecules often expressed on human tumors. (**A**) Schematic showing two key immune regulatory proteins expressed on the cell surface of tumor cells, CD47 and PD-L1, and the immune cells that recognize them. **(B)** Protein expression of CD47 and PD-L1 in murine primary MYC T-All before and after MYC inactivation. Tumors were harvested from primary MYC T-ALL transgenic animals 0 (MYC ON) or 4 days (MYC OFF) following MYC inactivation with Dox. Immunofluorescence staining of CD47 and PD-L1 (labeled in dark pink, DAPI counterstain) was performed. Images are representative of 3 different tumors per condition. Scale bar = 50 μm.

A

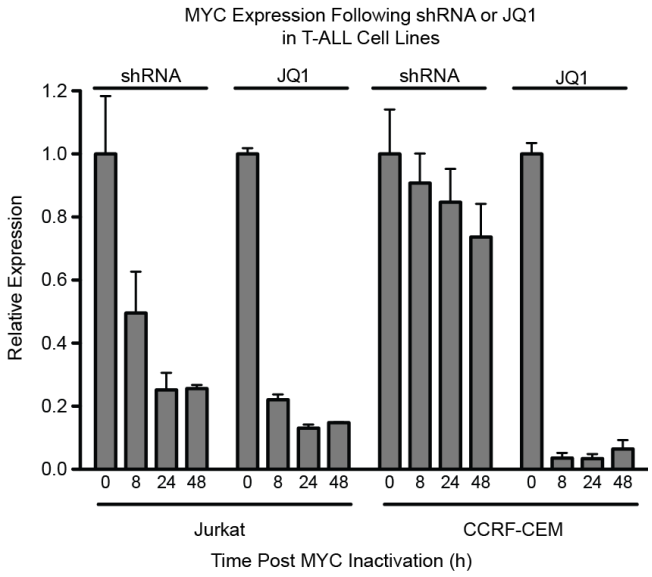

B

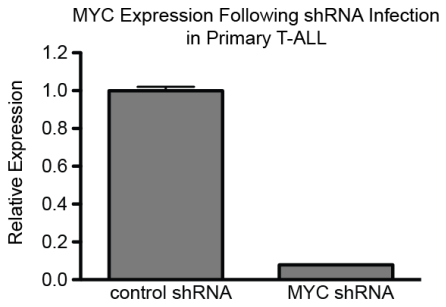

Fig. S2

MYC mRNA levels before and after treatment with shRNA against MYC or treatment with JQ1. MYC mRNA was measured by qPCR in human T-ALL cell lines (A, n=3) and primary human T-ALL (B, n=4) cells following MYC inhibition by shRNA or JQ1 treatment after the indicated number of hours (0-48 h for human T-ALL cell lines, 48 h for primary T-ALL).

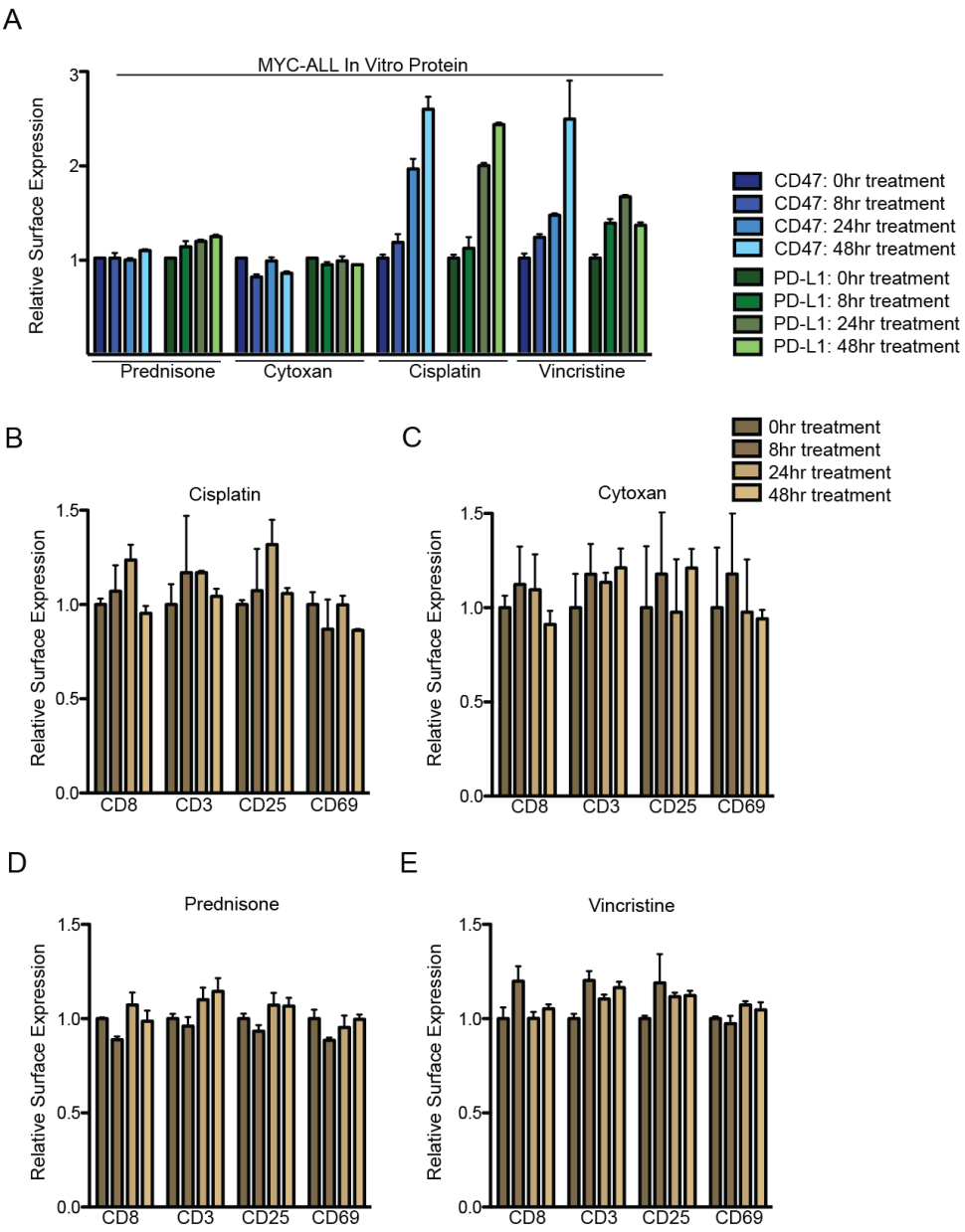

Fig. S3

Chemotherapy has no effect or increases the expression of CD47 or PD-L1 and has no effect on expression of CD8, CD3, CD25 or CD69. **(A)** CD47 (blue) and PD-L1 (green) protein levels in MYC T-ALL 4188 cells treated with prednisone, cytoxan, cisplatin, or vincristine (10 μM each) were quantified by flow cytometry MFI. Means ± SEM are shown, n=3. **(B-E)** CD3, CD8, CD25, and CD69 protein levels in MYC T-ALL 4188 cells treated as in **(A)** were quantified by flow cytometry. Means ± SEM are shown (n=3).

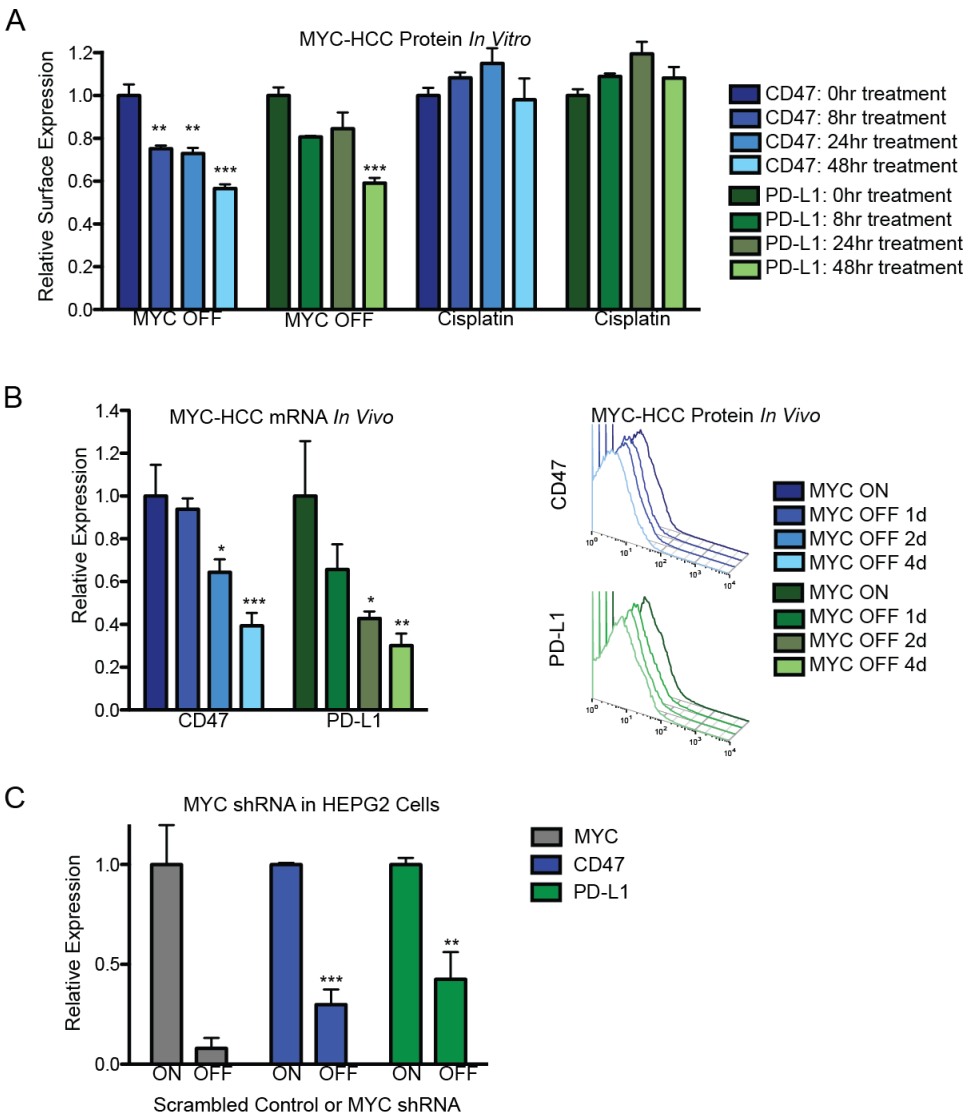

Fig. S4

MYC regulates the mRNA and protein expression of CD47 and PD-L1 in HCC. **(A)** CD47 (blue) and PD-L1 (green) protein levels in cells derived from mouse MYC-driven HCC, following MYC inactivation or chemotherapy treatment, were quantified by flow cytometry MFI (n=3). **(B)** CD47 (blue) and PD-L1 (green) mRNA levels were quantified by qPCR and protein levels were quantified by flow cytometry in primary tumors from mouse MYC-driven HCC, following MYC inactivation (n=3 tumors per condition). **(C)** MYC (gray), CD47 (blue), and PD-L1 (green) mRNA levels in human HEPG2 HCC cells were quantified by qPCR 48 h after MYC shRNA knockdown. n=3. Means ± SEM are shown.

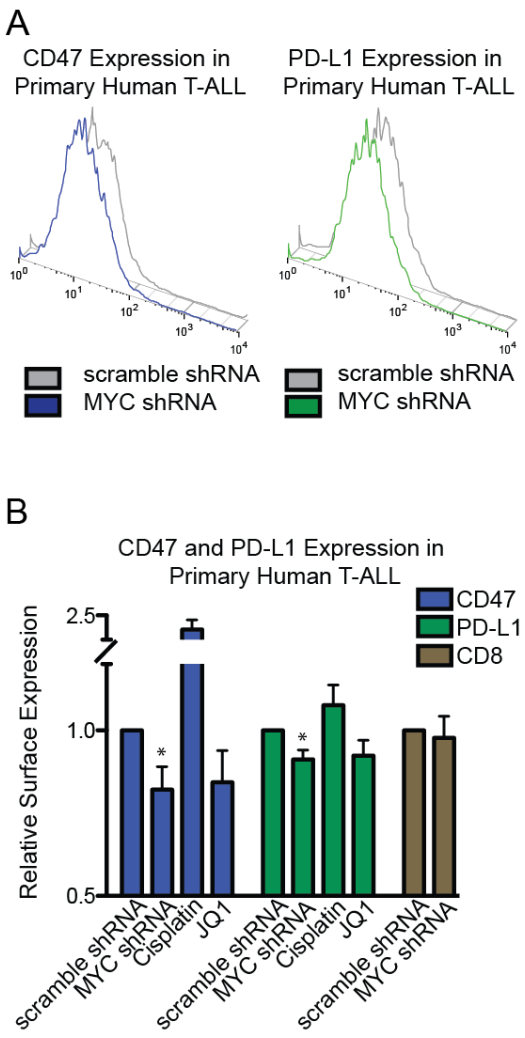

Fig. S5

MYC regulates expression of CD47 and PD-L1 in primary human T-ALL. **(A)** CD47 (blue) and PD-L1 (green) protein levels in primary human T-ALL tumor samples were quantified by flow cytometry, following 48 h treatment with control scramble shRNA or MYC-targeting shRNA. **(B)** CD47 (blue), PD-L1 (green), or CD8 (brown) protein levels in primary human T-ALL tumor samples were quantified by flow cytometry MFI, following 48 h treatment with control scramble shRNA or MYC-targeting shRNA, or treatment with 10 μM JQ1 or10 μM cisplatin (n=4 distinct patient samples). Means ± SEM are shown.

A

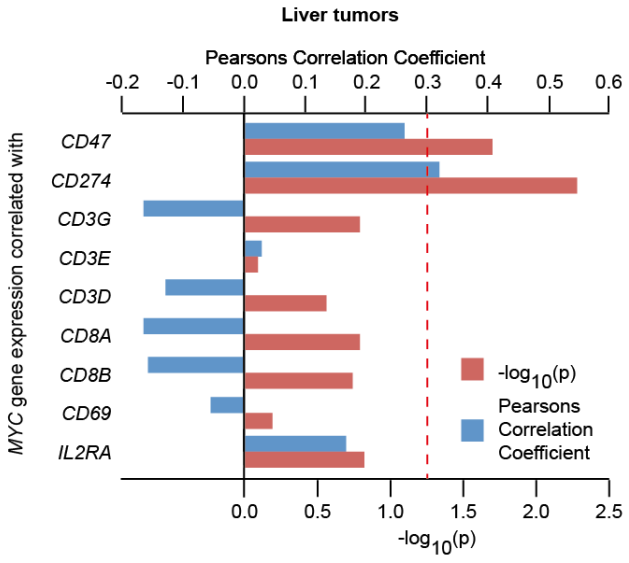

B

MYC gene expression correlated with	HCC (Wurmbach et al.)		RCC (Kort et al.)		CRC (Julien et al.)	
	Pearsons Correlation Coefficient	$-\log_{10}(p)$	Pearsons Correlation Coefficient	$-\log_{10}(p)$	Pearsons Correlation Coefficient	$-\log_{10}(p)$
CD47	0.264	1.70	0.455	4.60	0.268	2.43
CD274	0.320	2.28	0.176	0.92	na	na
CD3G	-0.166	0.80	0.331	2.54	-0.184	1.30
CD3E	0.028	0.09	0.432	4.15	-0.145	0.92
CD3D	-0.130	0.57	0.516	5.96	-0.143	0.89
CD8A	-0.164	0.80	0.187	1.00	0.007	0.03
CD8B	-0.158	0.74	0.180	0.96	0.004	0.01
CD69	-0.055	0.19	0.491	5.37	-0.171	1.15
IL2RA	0.167	0.82	-0.020	0.07	-0.173	1.22

Fig. S6

MYC expression correlates with CD47 and PD-L1 (CD274) expression in human tumors. **(A)** Correlation of MYC gene expression with the expression of several immune-related surface receptors in a dataset of human HCCs (n=75, (*52*)). The dashed red line indicates $P = 0.05$. **(B)** Three datasets of human HCC (n=75, *(52)*), RCC (n=79, *(53)*) and CRC (n=115, *(54)*) were analyzed for correlation of MYC expression with immune-related cell surface molecules. Pearsons correlation coefficients were determined using one representative probe for each gene („na“: no probe was detected for that gene) and *P*-values are given as negative common logarithm to the base 10.

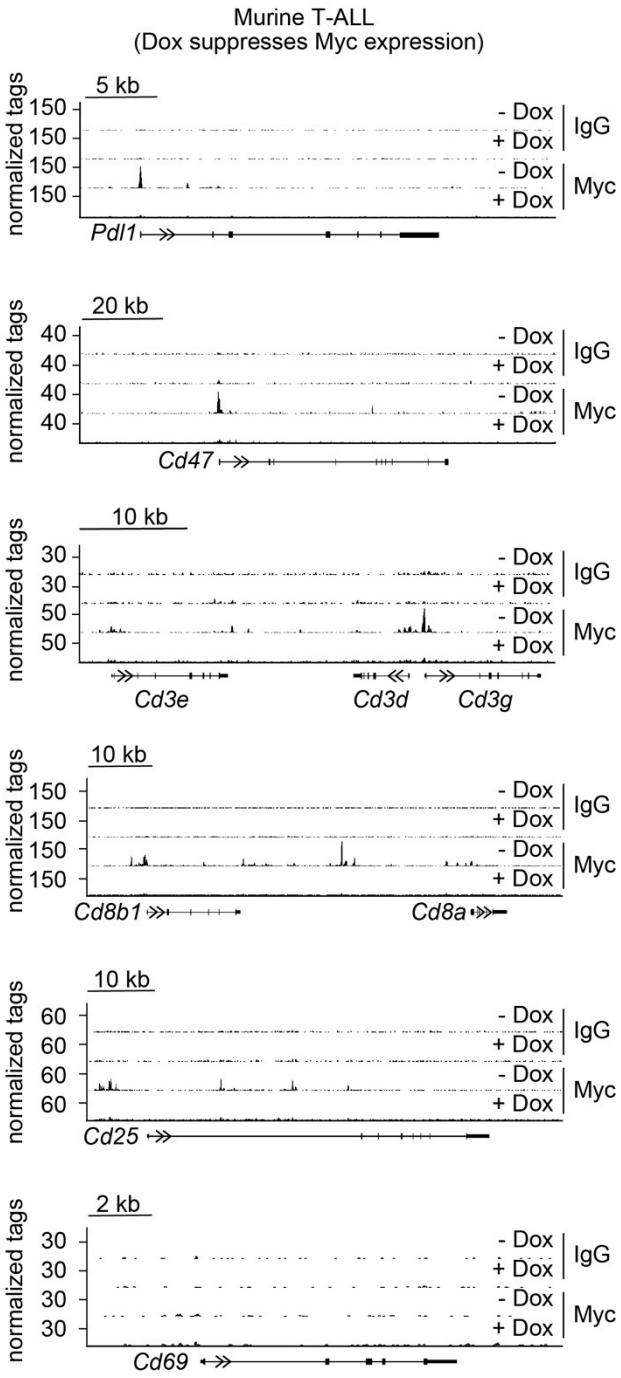

Fig. S7

MYC DNA binding in conditional transgenic mouse MYC T-ALL cells. ChIP-sequencing traces were generated from GSE44672 *(34)*. IgG was used as a negative control. Exons are represented as vertical bars, the UTR is represented by a black line, and arrows indicate the direction of transcription.

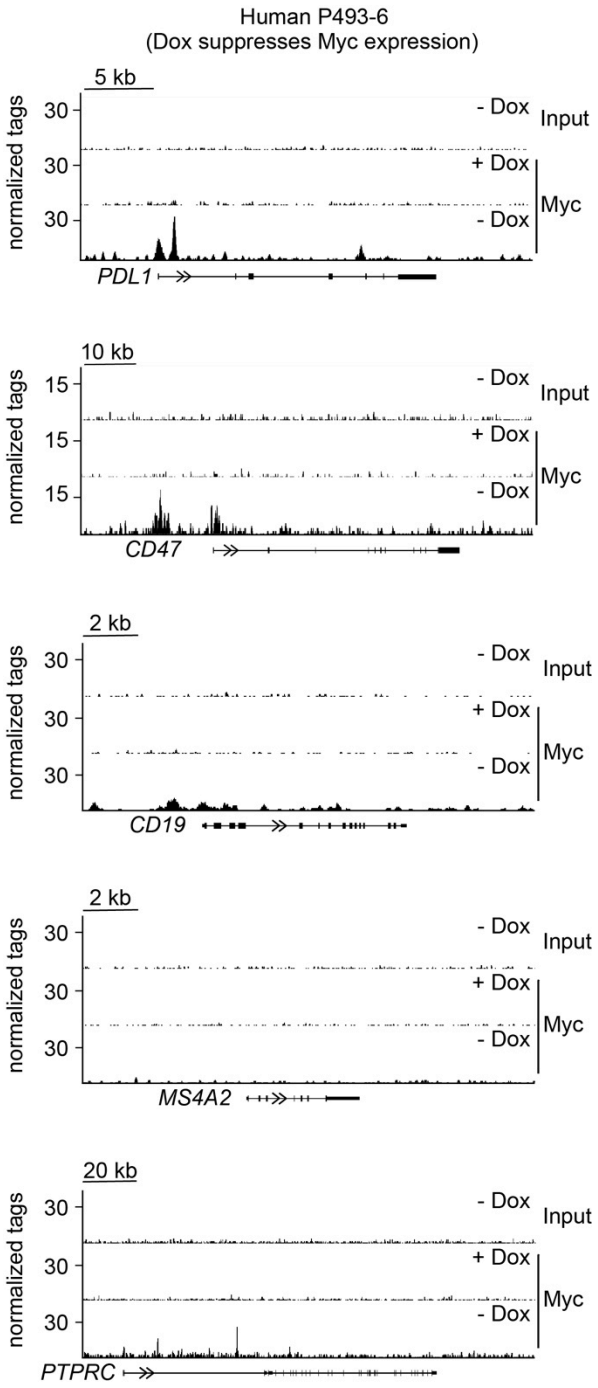

Fig. S8

MYC DNA binding in human P493-6 Burkitt lymphoma-like cells. Binding profiles were generated from GSE51004 *(38)*. Exons are represented as vertical bars, the UTR is represented by a black line, and arrows indicate the direction of transcription.

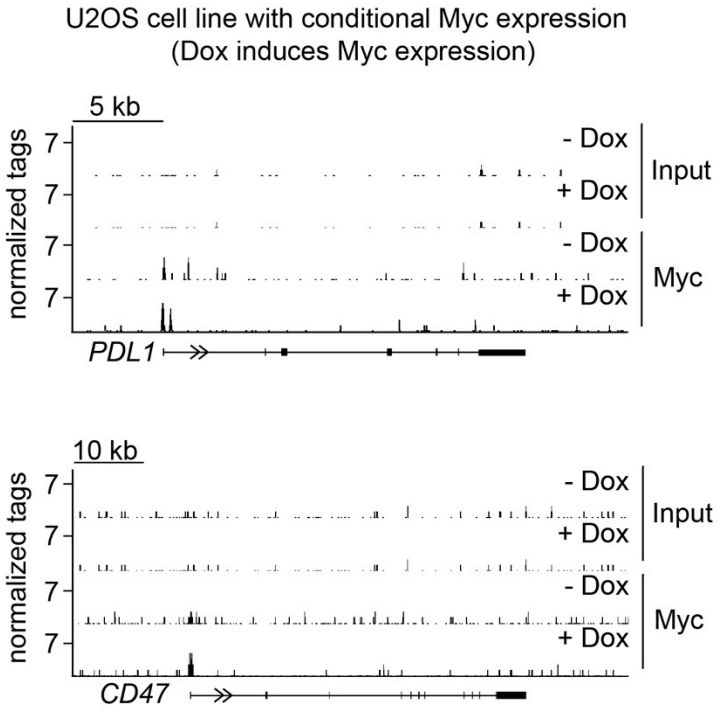

Fig. S9

MYC DNA binding in conditional MYC-driven U2OS cells. ChIP-sequencing traces were generated from GSE44672 *(34)*. Exons are represented as vertical bars, the UTR is represented by a black line, and arrows indicate the direction of transcription.

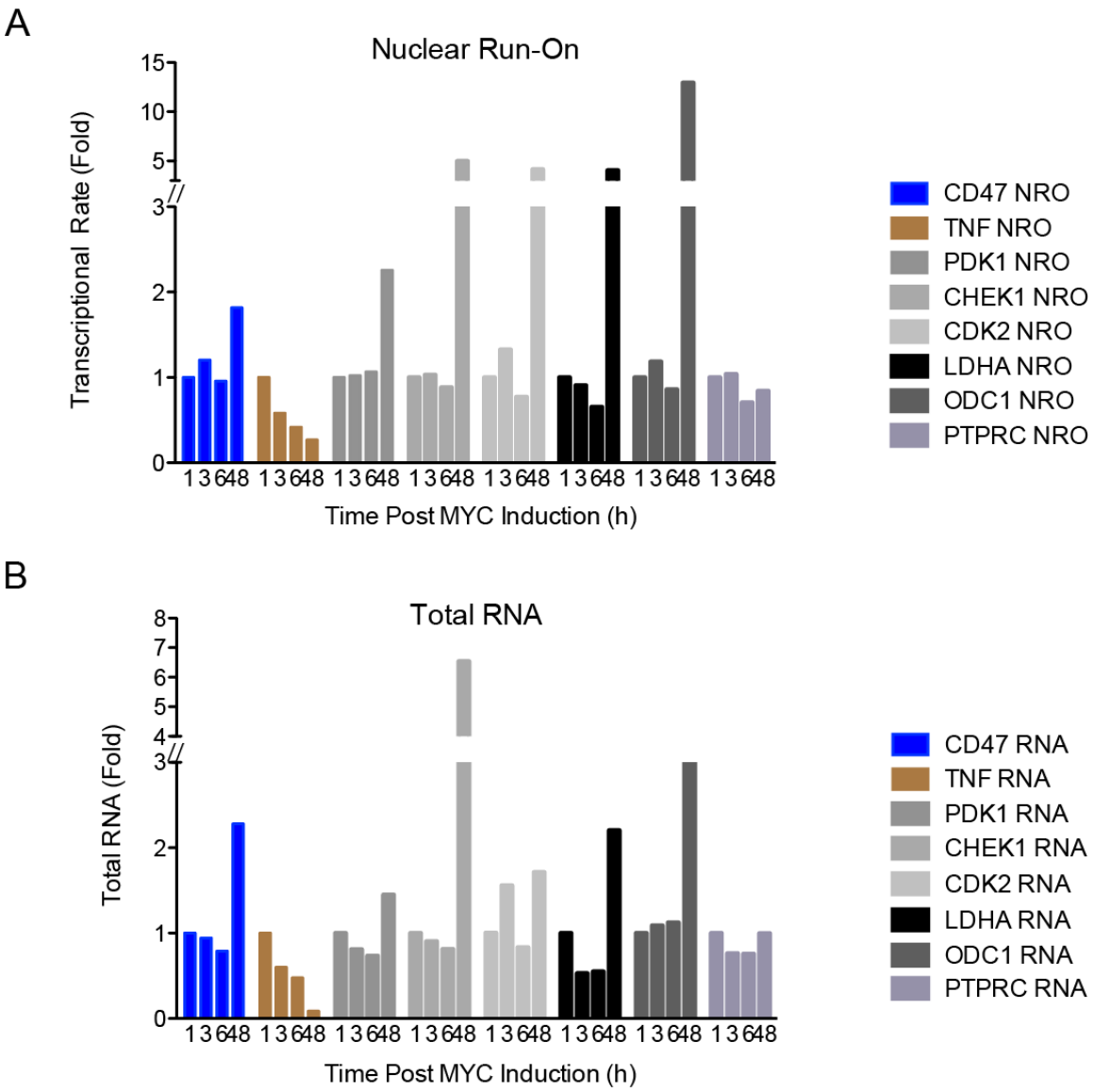

Fig. S10

Measurement of RNA by nuclear run-on analysis after MYC induction. **(A-B)** Nuclear run-on analysis of CD47, TNF, PDK1, CHEK1, CDK2, LDHA, ODC1, and PTPRC gene transcription following MYC activation in P493-6 cells.

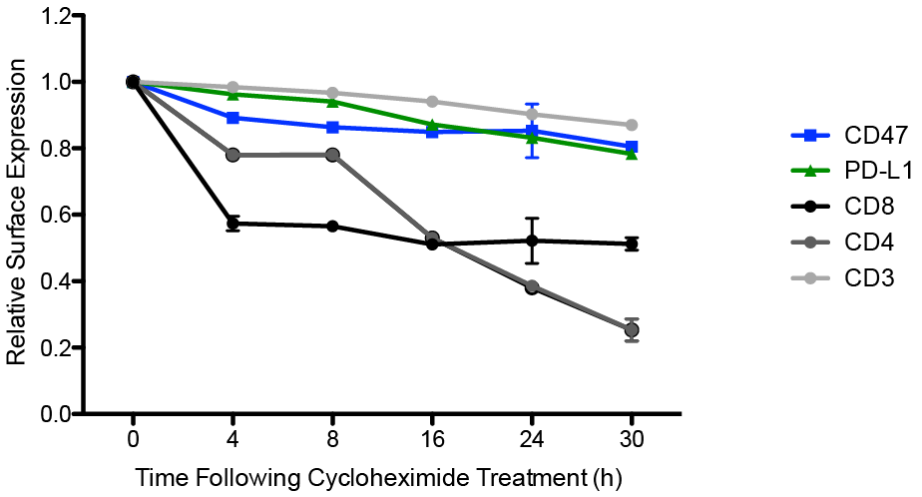

Fig. S11

Relative protein stability of immune surface receptors following cycloheximide treatment. MYC T-ALL 4188 cells were treated with 20 μg/mL cycloheximide and the relative surface expression of immune surface molecules was quantified by flow cytometry at the indicated time points (n=3). Means ± SEM are shown.

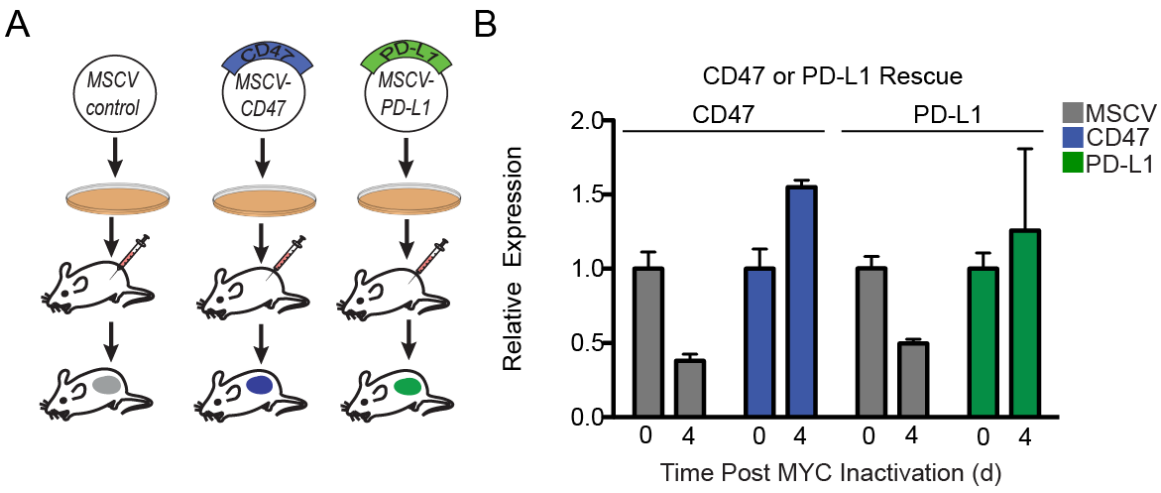

Fig. S12

General strategy for maintaining expression of CD47 or PD-L1 after MYC inactivation **(A)** Retroviral mediated expression of CD47 (blue) and PD-L1 (green) in MYC T-ALL 4188 cells. Empty MSCV retroviral vector (control) or retroviral vector containing either CD47 or PD-L1 cDNA was used to infect MYC T-ALL 4188 cells to maintain expression of CD47 or PD-L1 even upon MYC inactivation. **(B)** mRNA levels of CD47 and PD-L1 in transplanted control (gray) or constitutive CD47/PD-L1-expressing (colored) tumors at 0 and 4 days following MYC inactivation in WT mice (FVB strain) (n=3 tumors per condition). Means ± SEM are shown.

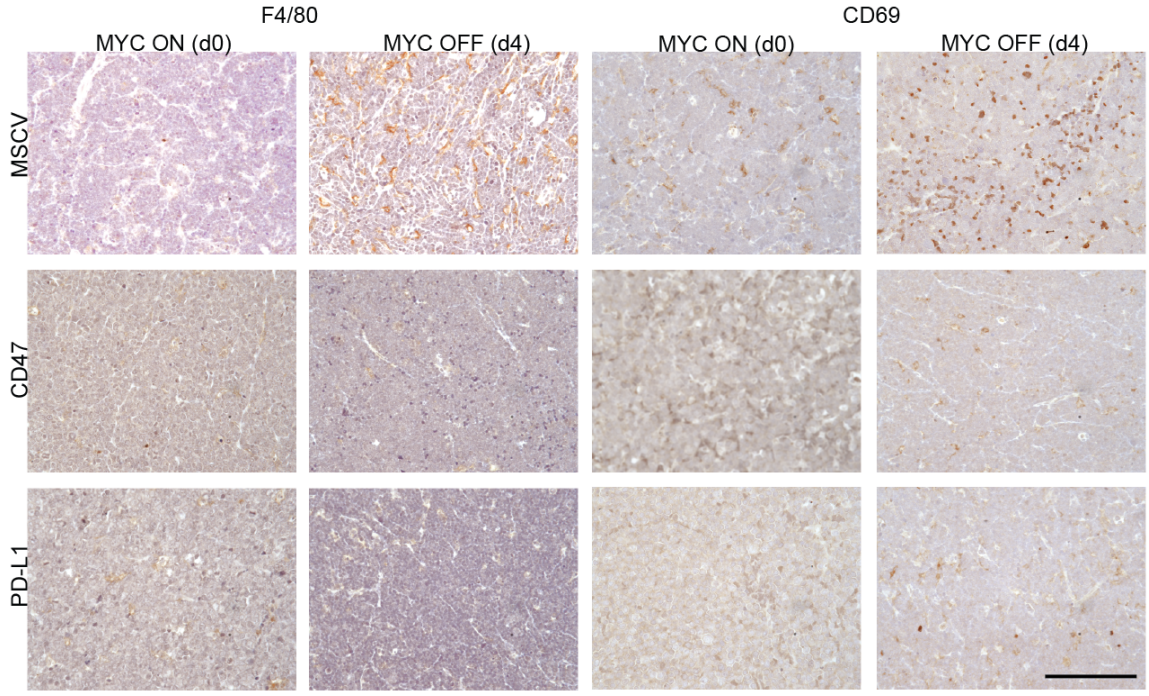

Fig. S13

Sustained expression of CD47 or PD-L1 inhibits the recruitment of immune cells following MYC inactivation. Immunohistochemistry of macrophages (F4/80) and activated lymphocytes (CD69) in control MSCV, CD47-expressing, and PD-L1-expressing tumors following MYC inactivation in WT FVB hosts. Images are representative of 3 distinct tumors and 3 images per tumor. Scale bar: 100 μm.

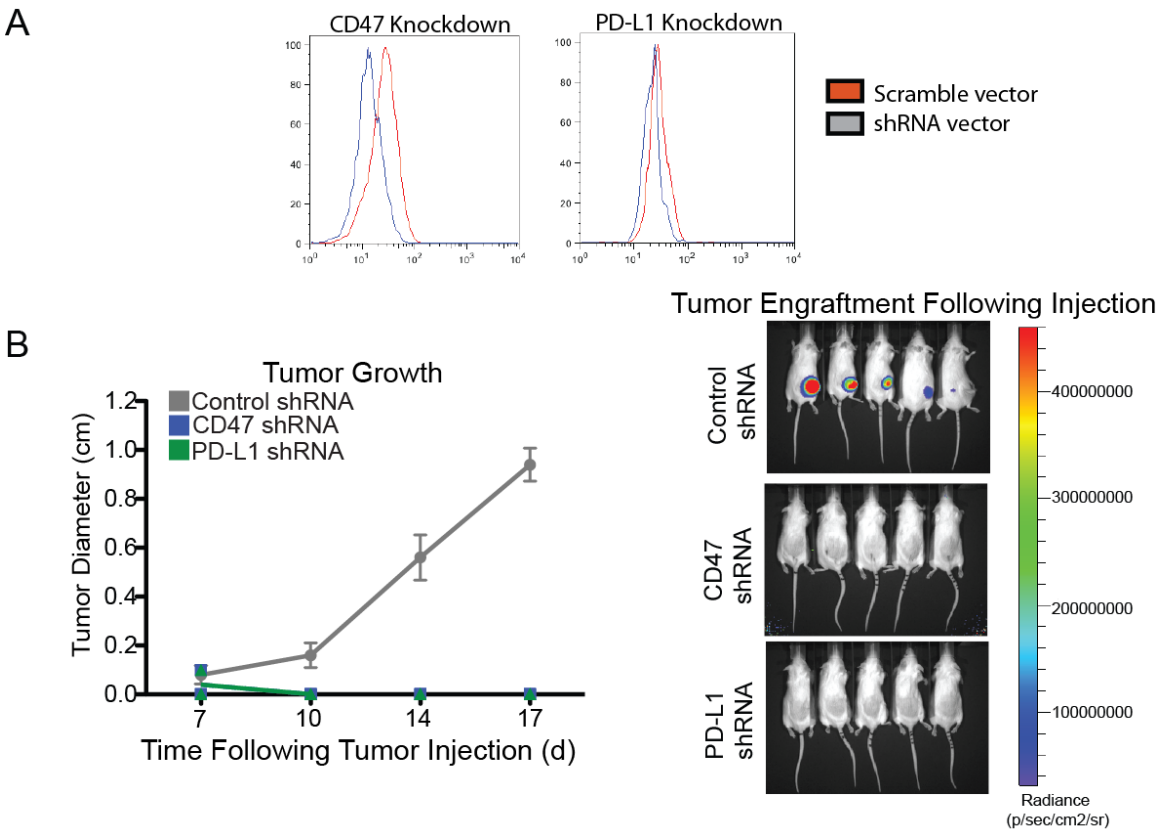

Fig. S14

The shRNA mediated reduced expression of CD47 or PD-L1 prevents tumor engraftment. **(A)** MYC T-ALL 4188 cells were infected with lentivirus carrying the control scrambled shRNA or shRNA targeting CD47 or PD-L1, and CD47 (left) or PD-L1 (right) surface protein expression was detected. **(B)** Representative mice with bioluminescence indicating tumor growth are shown 17 d after the injection of tumor cells expressing CD47- or PD-L1-targeting shRNA (right). Tumor diameters were measured by calipers and plotted as the mean ± SEM (left). n=5 mice per condition.

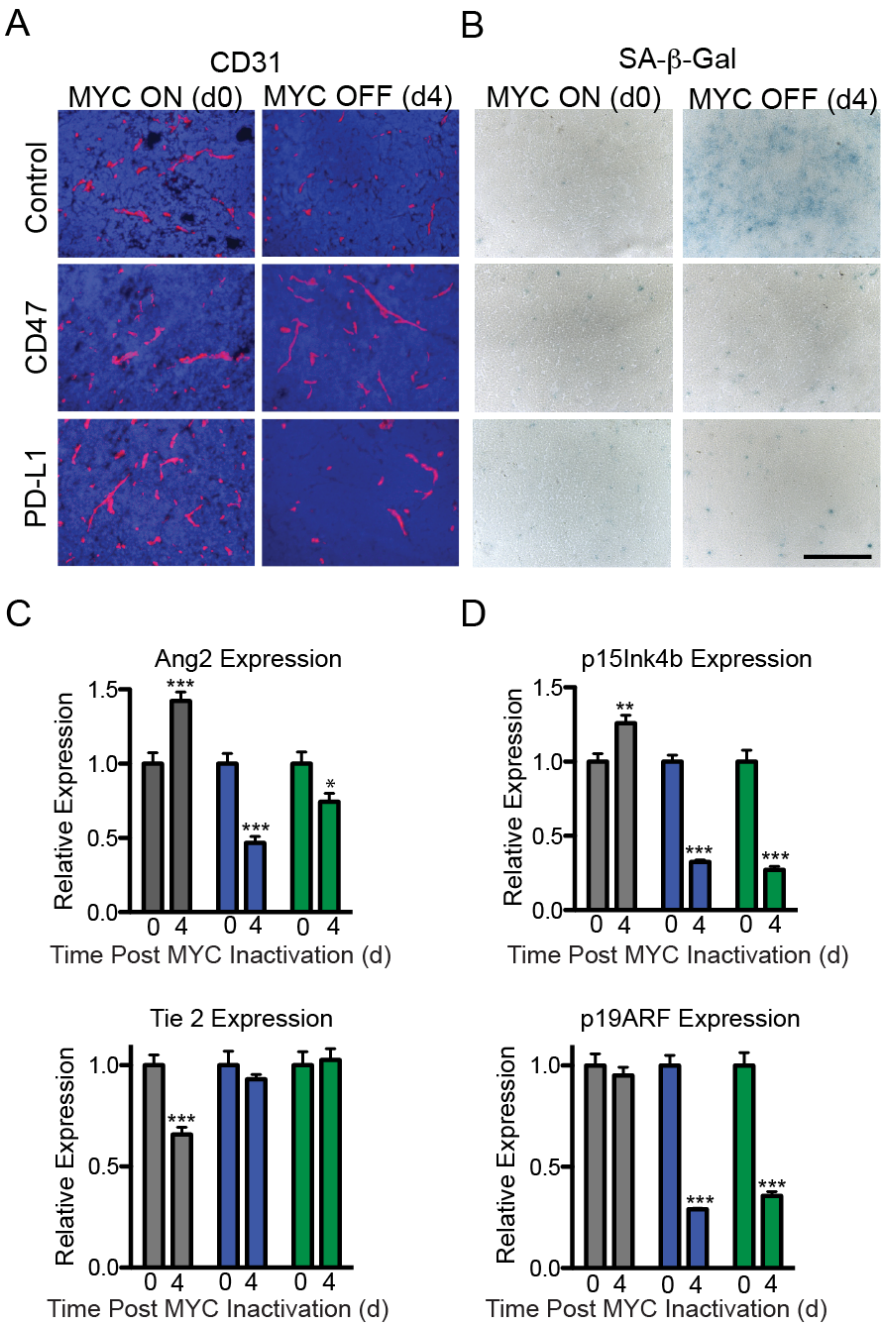

Fig. S15

Sustained expression of CD47 or PD-L1 alters angiogenesis and senescence. **(A)** Immunofluorescence of CD31 (detecting angiogenesis) in control, CD47-expressing, or PD-L1-expressing tumors (generated as described in Fig. S12) 0 or 4 d following MYC inactivation. Quantification is shown in Fig. 4E. **(B)** SA-β-gal (induction of senescence) staining of tumors described in (A). Quantification is shown in Fig. 4F. Scale bar: 100 μm. Images are representative of 3 distinct tumors and 3 images per tumor. Relative expression as measured by qPCR of **(C)** Ang2, Tie2, **(D)** p15Ink4b, and p19ARF in control (gray), CD47-expressing (blue), and PD-L1-expressing (green) tumors before (d0) and after MYC inactivation (d4). Graphs are presented as the mean ± SEM (n=3 distinct tumors per condition).

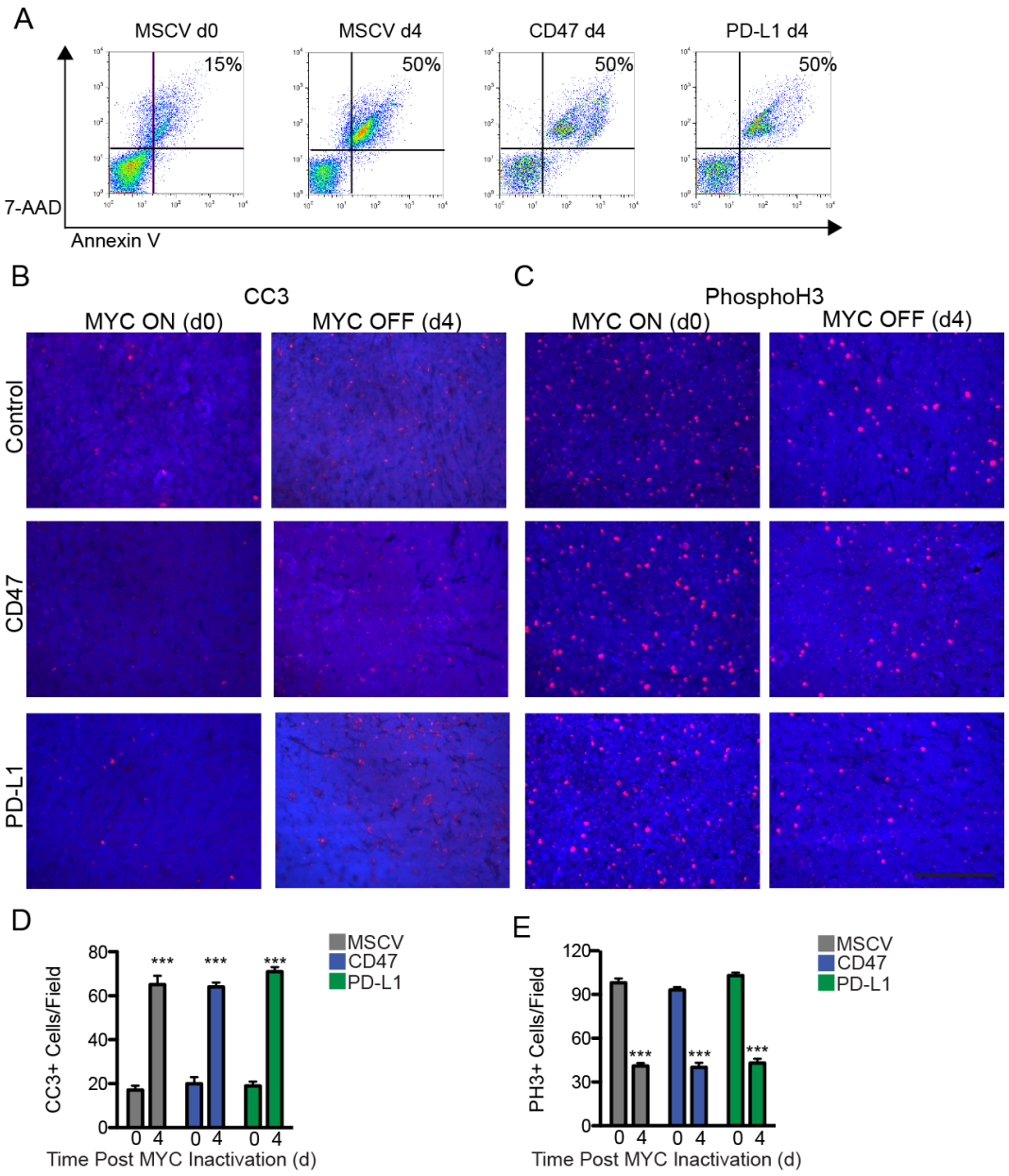

Fig. S16

Sustained expression of CD47 or PD-L1 does not affect apoptosis or proliferation arrest upon MYC inactivation. **(A)** Annexin V and 7-AAD were labeled in MYC T-ALL 4188 cells expressing control pMSCV, CD47, or PD-L1 following MYC inactivation *in vitro* and detected by flow cytometry (n=3). Cells in the upper right quadrant represent the percentage of apoptotic cells. **(B)** CC3 immunofluorescence detecting apoptosis (dark pink stain, DAPI counterstain) of tumors as indicated in Fig 4. Scale bar = 100 μm. Images are representative of 3 distinct tumors and 3 images per tumor. **(C)** PH3 immunofluorescence detecting cells in metaphase (dark pink stain, DAPI counterstain) of tumors as indicated in Fig 4. **(D-E)** Quantification of CC3 **(D)** and PH3 **(E)** immunofluorescence. Graphs are presented as the mean ± SEM (n=3 distinct tumors per condition). The y axis denotes the number of positively staining cells per field.

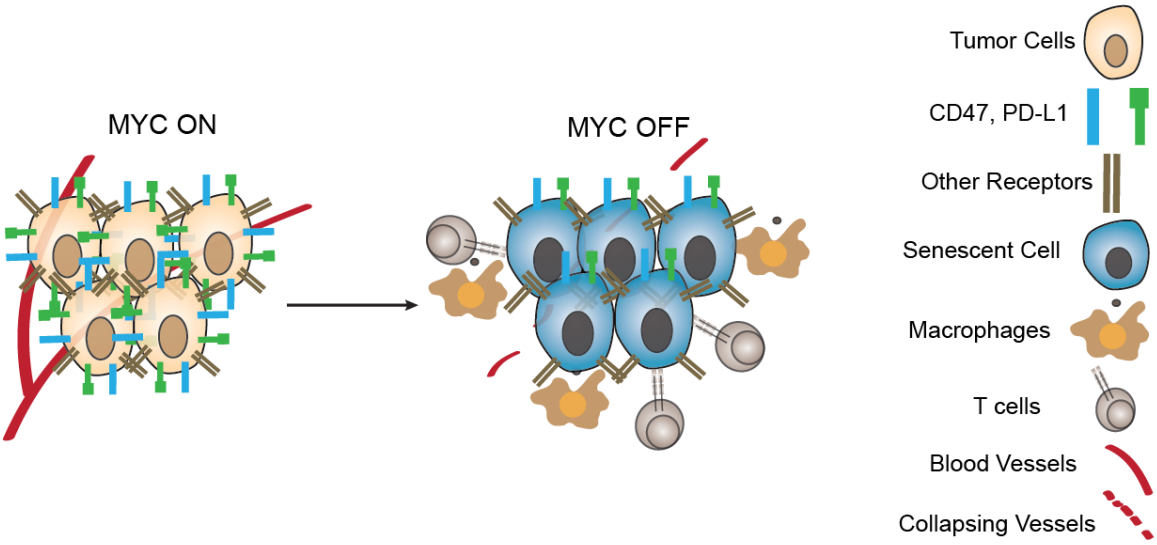

Fig. S17

MYC regulates the immune response against tumor cells via CD47 and PD-L1. Model demonstrating the regulation of immunological checkpoints in MYC-driven tumors. Following MYC inactivation, the expression of CD47 and PD-L1 is reduced, leading to an immune response and the subsequent induction of senescence and shutdown of angiogenesis.

Supplemental Table 1

Transgenic MYC For	CTGCGACGAGGAGGAGAACT
Transgenic MYC Rev	GGCAGCAGCTCGAATTTCTT
Ang2 For	AGCAGATTTTGGATCAGACCAG
Ang2 Rev	GCTCCTTCATGGACTGTAGCTG
Tie2 For	CGGCTTAGTTCTCTGTGGAGTC
Tie2 Rev	GGCATCAGACACAAGAGGTAGG
p15Ink4b For	TCTTGGATCTCCACAAGC
p15Ink4b Rev	CTCCAGGTTTCCCATTTAC
p19ARF For	GTCGCAGGTTCTTGGTCACT
p19ARF Rev	ATCGCACGAACTTCACCAA
CD47 For	TGCGGTTCAGCTCAACTACTG
CD47 Rev	GCTTTGCGCCTCCACATTAC
PD-L1 For	GCTCCAAAGGACTTGTACGTG
PD-L1 Rev	TGATCTGAAGGGCAGCATTTC
UBC For	AGCCCAGTGTTACCACCAAG
UBC Rev	ACCCAAGAACAAGCACAAGG
hCD47 For	GGCAATGACGAAGGAGGTTA
hCD47 Rev	ATCCGGTGGTATGGATGAGA
hPD-L1 For	GGCATTTGCTGAACGCAT
hPD-L1 Rev	CAATTAGTGCAGCCAGGT

Table S1.
Primer sequences used for qPCR analysis of mRNA expression.

REFERENCES AND NOTES

1. D. W. Felsher, J. M. Bishop, Reversible tumorigenesis by MYC in hematopoietic lineages. *Molecular cell* **4**, 199-207 (1999).
2. M. Jain *et al.*, Sustained loss of a neoplastic phenotype by brief inactivation of MYC. *Science* **297**, 102-104 (2002).
3. C. M. Shachaf *et al.*, MYC inactivation uncovers pluripotent differentiation and tumour dormancy in hepatocellular cancer. *Nature* **431**, 1112-1117 (2004).
4. C. H. Wu *et al.*, Cellular senescence is an important mechanism of tumor regression upon c-Myc inactivation. *Proceedings of the National Academy of Sciences of the United States of America* **104**, 13028-13033 (2007).
5. V. M. Sharma *et al.*, Notch1 contributes to mouse T-cell leukemia by directly inducing the expression of c-myc. *Molecular and cellular biology* **26**, 8022-8031 (2006).
6. A. P. Weng *et al.*, c-Myc is an important direct target of Notch1 in T-cell acute lymphoblastic leukemia/lymphoma. *Genes & development* **20**, 2096-2109 (2006).
7. D. Marinkovic, T. Marinkovic, B. Mahr, J. Hess, T. Wirth, Reversible lymphomagenesis in conditionally c-MYC expressing mice. *International journal of cancer. Journal international du cancer* **110**, 336-342 (2004).
8. L. Hennighausen, R. J. Wall, U. Tillmann, M. Li, P. A. Furth, Conditional gene expression in secretory tissues and skin of transgenic mice using the MMTV-LTR and the tetracycline responsive system. *Journal of cellular biochemistry* **59**, 463-472 (1995).
9. S. Pelengaris, M. Khan, G. Evan, c-MYC: more than just a matter of life and death. *Nature reviews. Cancer* **2**, 764-776 (2002).
10. C. M. D'Cruz *et al.*, c-MYC induces mammary tumorigenesis by means of a preferred pathway involving spontaneous Kras2 mutations. *Nature medicine* **7**, 235-239 (2001).
11. G. H. Fisher *et al.*, Induction and apoptotic regression of lung adenocarcinomas by regulation of a K-Ras transgene in the presence and absence of tumor suppressor genes. *Genes & development* **15**, 3249-3262 (2001).
12. C. S. Huettner, P. Zhang, R. A. Van Etten, D. G. Tenen, Reversibility of acute B-cell leukaemia induced by BCR-ABL1. *Nature genetics* **24**, 57-60 (2000).
13. K. Rakhra *et al.*, CD4(+) T cells contribute to the remodeling of the microenvironment required for sustained tumor regression upon oncogene inactivation. *Cancer cell* **18**, 485-498 (2010).
14. S. Giuriato *et al.*, Sustained regression of tumors upon MYC inactivation requires p53 or thrombospondin-1 to reverse the angiogenic switch. *Proceedings of the National Academy of Sciences of the United States of America* **103**, 16266-16271 (2006).
15. F. Balkwill, A. Mantovani, Inflammation and cancer: back to Virchow? *Lancet* **357**, 539-545 (2001).
16. L. Gattinoni, D. J. Powell, Jr., S. A. Rosenberg, N. P. Restifo, Adoptive immunotherapy for cancer: building on success. *Nature reviews. Immunology* **6**, 383-393 (2006).
17. J. Galon *et al.*, Towards the introduction of the 'Immunoscore' in the classification of malignant tumours. *The Journal of pathology* **232**, 199-209 (2014).
18. A. Shanker *et al.*, CD8 T cell help for innate antitumor immunity. *J Immunol* **179**, 6651-6662 (2007).
19. A. Corthay *et al.*, Primary antitumor immune response mediated by CD4+ T cells. *Immunity* **22**, 371-383 (2005).

20. Z. Qin, T. Blankenstein, CD4+ T cell--mediated tumor rejection involves inhibition of angiogenesis that is dependent on IFN gamma receptor expression by nonhematopoietic cells. *Immunity* **12**, 677-686 (2000).
21. A. T. Parsa *et al.*, Loss of tumor suppressor PTEN function increases B7-H1 expression and immunoresistance in glioma. *Nature medicine* **13**, 84-88 (2007).
22. S. L. Topalian, C. G. Drake, D. M. Pardoll, Targeting the PD-1/B7-H1(PD-L1) pathway to activate anti-tumor immunity. *Current opinion in immunology* **24**, 207-212 (2012).
23. F. Tsushima *et al.*, Interaction between B7-H1 and PD-1 determines initiation and reversal of T-cell anergy. *Blood* **110**, 180-185 (2007).
24. S. Jaiswal *et al.*, CD47 is upregulated on circulating hematopoietic stem cells and leukemia cells to avoid phagocytosis. *Cell* **138**, 271-285 (2009).
25. R. Majeti *et al.*, CD47 is an adverse prognostic factor and therapeutic antibody target on human acute myeloid leukemia stem cells. *Cell* **138**, 286-299 (2009).
26. P. Sharma, J. P. Allison, Immune checkpoint targeting in cancer therapy: toward combination strategies with curative potential. *Cell* **161**, 205-214 (2015).
27. M. P. Chao *et al.*, Therapeutic antibody targeting of CD47 eliminates human acute lymphoblastic leukemia. *Cancer research* **71**, 1374-1384 (2011).
28. S. R. Woo, L. Corrales, T. F. Gajewski, Innate immune recognition of cancer. *Annual review of immunology* **33**, 445-474 (2015).
29. L. Galluzzi *et al.*, Classification of current anticancer immunotherapies. *Oncotarget* **5**, 12472-12508 (2014).
30. P. Filippakopoulos *et al.*, Selective inhibition of BET bromodomains. *Nature* **468**, 1067-1073 (2010).
31. B. Homet Moreno, G. Parisi, L. Robert, A. Ribas, Anti-PD-1 therapy in melanoma. *Seminars in oncology* **42**, 466-473 (2015).
32. Z. Nie *et al.*, c-Myc is a universal amplifier of expressed genes in lymphocytes and embryonic stem cells. *Cell* **151**, 68-79 (2012).
33. C. Y. Lin *et al.*, Transcriptional amplification in tumor cells with elevated c-Myc. *Cell* **151**, 56-67 (2012).
34. S. Walz *et al.*, Activation and repression by oncogenic MYC shape tumour-specific gene expression profiles. *Nature* **511**, 483-487 (2014).
35. K. E. Wiese *et al.*, The role of MIZ-1 in MYC-dependent tumorigenesis. *Cold Spring Harbor perspectives in medicine* **3**, a014290 (2013).
36. Y. Li, P. S. Choi, S. C. Casey, D. L. Dill, D. W. Felsher, MYC through miR-17-92 suppresses specific target genes to maintain survival, autonomous proliferation, and a neoplastic state. *Cancer cell* **26**, 262-272 (2014).
37. M. Schuhmacher *et al.*, Control of cell growth by c-Myc in the absence of cell division. *Current biology : CB* **9**, 1255-1258 (1999).
38. A. Sabo *et al.*, Selective transcriptional regulation by Myc in cellular growth control and lymphomagenesis. *Nature* **511**, 488-492 (2014).
39. R. D. Schreiber, L. J. Old, M. J. Smyth, Cancer immunoediting: integrating immunity's roles in cancer suppression and promotion. *Science* **331**, 1565-1570 (2011).
40. G. Dranoff, Experimental mouse tumour models: what can be learnt about human cancer immunology? *Nature reviews. Immunology* **12**, 61-66 (2012).

41. D. Mittal, M. M. Gubin, R. D. Schreiber, M. J. Smyth, New insights into cancer immunoediting and its three component phases--elimination, equilibrium and escape. *Current opinion in immunology* **27**, 16-25 (2014).
42. E. Wolf, C. Y. Lin, M. Eilers, D. L. Levens, Taming of the beast: shaping Myc-dependent amplification. *Trends in cell biology* **25**, 241-248 (2015).
43. M. Waclavicek *et al.*, T cell stimulation via CD47: agonistic and antagonistic effects of CD47 monoclonal antibody 1/1A4. *J Immunol* **159**, 5345-5354 (1997).
44. M. N. Avice, M. Rubio, M. Sergerie, G. Delespesse, M. Sarfati, Role of CD47 in the induction of human naive T cell anergy. *J Immunol* **167**, 2459-2468 (2001).
45. S. Kaur *et al.*, Thrombospondin-1 signaling through CD47 inhibits self-renewal by regulating c-Myc and other stem cell transcription factors. *Scientific reports* **3**, 1673 (2013).
46. I. B. Weinstein, A. Joe, Oncogene addiction. *Cancer research* **68**, 3077-3080; discussion 3080 (2008).
47. O. Bruserud, N. Glenjen, A. Ryningen, E. Ulvestad, In vitro culture of human acute lymphoblastic leukemia (ALL) cells in serum-free media; a comparison of native ALL blasts, ALL cell lines and virus-transformed B cell lines. *Leukemia research* **27**, 455-464 (2003).
48. J. W. Nicol, G. A. Helt, S. G. Blanchard, Jr., A. Raja, A. E. Loraine, The Integrated Genome Browser: free software for distribution and exploration of genome-scale datasets. *Bioinformatics* **25**, 2730-2731 (2009).
49. J. Fan *et al.*, Time-dependent c-Myc transactomes mapped by Array-based nuclear run-on reveal transcriptional modules in human B cells. *PloS one* **5**, e9691 (2010).
50. J. Fan *et al.*, Array-based nuclear run-on analysis. *Methods in molecular biology* **809**, 505-517 (2012).
51. H. Ji *et al.*, Cell-type independent MYC target genes reveal a primordial signature involved in biomass accumulation. *PloS one* **6**, e26057 (2011).
52. E. Wurmbach *et al.*, Genome-wide molecular profiles of HCV-induced dysplasia and hepatocellular carcinoma. *Hepatology* **45**, 938-947 (2007).
53. E. J. Kort *et al.*, The E2F3-Oncomir-1 axis is activated in Wilms' tumor. *Cancer research* **68**, 4034-4038 (2008).
54. S. Julien *et al.*, Characterization of a large panel of patient-derived tumor xenografts representing the clinical heterogeneity of human colorectal cancer. *Clinical cancer research : an official journal of the American Association for Cancer Research* **18**, 5314-5328 (2012).